Computer Assisted Mechanics & Engineering Sciences, 1: 95–113, 1994.

Elasto-plastic constitutive interface model for an axisymmetric contact problem

Ryszard Buczkowski
Technical University of Szczecin, Poland

Michał Kleiber
Institute of Fundamental Technological Research, Polish Academy of Sciences, Warsaw, Poland

(Received June 6, 1994)

A solution to plane and axisymmetric elasto-plastic contact problem with linear hardening of contacting bodies, taking into account microstructural features of the contact zone is presented. A new quadratic-isoparametric contact element involving the irreversible nature of friction is developed. An incremental constitutive friction law, analogous to the classical theory of plasticity, is used. Several numerical examples are considered. The influence of parameters defining the contact stiffness interface on the distribution of displacements and stresses on the contact surface is discussed.

1. INTRODUCTION

Machine tools are not generally manufactured as one continuos fabrication. Such constructions necessitate connections between the basic elements of the machine and these can be classified as fixed (e.g. bolted or flanged) joints and sliding (e.g. shrink-fitted or conical) joints. Machine tool rigidity is defined by both rigidity of the parts of machine tool structure and joint stiffness. The stiffness of joints, defined by the deflection at the interface of their elements, is of great importance for the precision machine tool. The deflections of joints are of great importance in machine tools due to the following reasons:

- calculation of the normal stiffness and pressure distribution in the joints under the assumption that the structural components are rigid (perfectly smooth bodies) gives the normal displacements several times smaller than those obtained with a normal contact stiffness; the effect of roughness increases with decreasing contact pressure,
- the surface roughness of the joint has a significant effect on the contact stiffness as it determines the global behaviour of the machine joint,
- the contact areas are large so that deviations from ideal shape are inevitable (flatness deviations, ovality, etc.),
- the elastic (reversible) tangential displacements take place within the specific range of loads. For a further increase of the shear force exceeding the limit, the resulting displacements are elasto-plastic followed by macro-slip. Irreversible (plastic) tangential displacements give the rise to friction corrosion and can result in early wear of the machine.

Most numerical investigations in the field of contact mechanics have been performed for the classical Coulomb's law excluding local micromechanical phenomena within the contact interface.

Much of the work carried out on establishing the characteristics of machine tool joints has concentrated on the normal compliance of contacting surfaces and its dependence on surface topography, hardness, interface pressure and materials.

Recently, the frictional phenomena have been considered within the framework of the theory of plasticity. Elasto-plastic relations for frictional problems have been proposed by Fredriksson [12], Michałowski and Mróz [26], Curnier [10], Cheng and Kikuchi [7,8], Plesha [28], Plesha et al. [29], Wriggers [40] and Wriggers, Vu Van and Stein [41]. The assumption that the normal contact stresses are known implies an associated sliding rule, see e.g. Fredriksson [12], Cheng and Kikuchi [7,8]. If no assumption of the contact normal pressure in the contact area is made a non-associated slip rule results [11, 14, 18, 20, 24, 26, 28, 29, 31, 40, 43] which leads to a non-symmetric tangent stiffness matrix, and a finite element solver for unsymmetric matrices has to be adopted. In order to take into account the influence of roughness upon the contact pressure and shear stress distribution different analysis methods may be used. Some of the methods are based on the discrete model in which the asperities have simple geometrical forms, e.g. that of a cylinder, wedge, sphere, etc. In these methods the analysis resolves itself into the investigation of influence of the microgeometrical morphology and mechanical material properties on the interaction of the contacting rough surfaces [35,37,42]. Another approach to the analysis of the contact problem consists in the experimental determination of the load-displacement characteristics for real surfaces and the substitution of simple mathematical expressions for them. Such a method has been employed in the present study. Back, Burdekin and Cowley [1,2] were the first who used experimentally determined parameters (normal compliance condition) in the calculation of examples of simple machine tool joints by the finite element method. Kops and Abrams [23] discussed the additional effect of the shear and normal stiffness of the interface on the thermal deformation of machine tool structure. An effective model of frictional interface behaviour was proposed by Villanueva-Leal and Hinduja [39]. These authors were first to successfully employ the incremental formulation to solve 3D-bolted joints with both the normal and tangential contact stiffness. The values of shear forces were constrainted by the Coulomb law of friction. The elasto-plastic contact problem with the contact stiffness was presented by Bloch and Orobinski [4] and Buczkowski and Kleiber [5]. Cheng and Kikuchi [7,8] presented an elasto-plastic problem of unilateral contact in which the elasto-plastic law was extended to large deformations typical of some metal forming processes. Wriggers [40] and Wriggers, Vu-Van and Stein [41] took advantage of the expressions describing the nonlinear behaviour of the contact surface in the normal and tangential direction. They reported the solution to two-dimensional static and dynamic problems under large deformations and a nonlinear friction law.

The present study deals with the solution to a plane stress and axisymmetric elastic-plastic contact problem with linear hardening of the basic elements taking into account elasto-plastic interface model. The nonlinear problem is solved by using an incremental-iterative Newton-Raphson procedure. The present solution method is illustrated by three numerical examples. The structure is discretized by eight node quadratic elements of the serendipity family. The elasto-plastic behaviour at the contact interface is designated below by (e-p) whereas the elasto-plastic deformation of the contacting bodies A and B by (E-P).

2. Modelling of interface surface roughness

2.1. Normal behaviour

Many researchers have observed that in the presence of surface asperities the relationship between the interface pressure and the approach of the surfaces in contact can be expressed by the following nonlinear power equation [25]

$$u_N = c_N p_N^m \tag{1}$$

where u_N is the deflection of the asperities, p_N is the mean interface pressure and the parameters c_N and m are coefficients depending upon the materials in contact, matching process, height of the asperities, relative orientation at the surface layers, hardness, flatness deviation and size of the contact area.

2.2. Normal stiffness

The use of the incremental method is unavoidable because it makes it possible to gradually adjust the slope so that the resultant curve $u_N - p_N$ follows the experimental curve desired. The stiffness value corresponds to the slope of the pressure-deflection characteristics at the working interface pressure. The power law relationship in Eq. (1) gives the stiffness per unit area as

$$k_N = \frac{p_N^{(1-m)}}{c_N m}. \tag{2}$$

A calculation method of the contact stiffness for the first and the next loading steps is given in Villanueva-Leal and Hinduja [39]. For the description of loading and unloading processes Eq. (2) applies with different values of the coefficients c_N and m.

2.3. Tangential behaviour

In addition to the normal loads the joint may be subjected to a tangential loading. The behaviour of the interface loaded in the tangential direction was reviewed in Buczkowski and Kleiber [5]. The elastic displacement takes place within the specific range of loads. For a further increase in the shear force above the limit the resulting displacements are elasto-plastic followed by a macro-slip. The plastic displacements of the asperities and macro-slip (slip displacements) are difficult to separate so that it is convenient to combine them into plastic (irrecoverable) displacements. It was found experimentally in Back et al. [2] that the shear stiffness depended upon the surface finish and it was decreasing with the decrease of the normal pressure. The relationship between the shear stiffness and the normal interface pressure in the elastic range was presented as

$$k_T^e = \frac{p_N^S}{R} \tag{3}$$

where S and R are parameters dependent upon both the materials and the surface finish [2].

In view of the results of Fredriksson [12] the normalized coefficient of friction may be related to the irrevesible (plastic) displacement as

$$\frac{\mu_F}{\mu_m} = 1 - (1-\beta)\exp\left(-n\overline{u_T^p}\right) \tag{4}$$

where μ_m is macroscopic (or static) coefficient of friction, β defines the initial coefficient of friction, n is the degree of slip hardening and $\overline{u_T^p} = \sqrt{\mathbf{u}_T^p \mathbf{u}_T^p} \equiv \|\mathbf{u}_T^p\|$ is the effective sliding (or accumulated plastic) displacement. The parametres n and β should be determined experimentally.

2.4. Calculation of tangential contact stresses

The basic characteristics of the contact problem model is the form of its sliding function F, which is specified in terms of the contact stresses $\mathbf{p}_T$ and p_N. We assume that there exists a generalized Coulomb isotropic slip function

$$F(\mathbf{p}_T, p_N, \mu_F) = \|\mathbf{p}_T\| + \mu_F p_N, \qquad p_N < 0, \tag{5}$$

where the normal stress component is given by $\mathbf{p}_N = (\mathbf{n} \otimes \mathbf{n})\mathbf{p} = (\mathbf{p}\mathbf{n})\mathbf{n} \equiv p_N\mathbf{n}$, the tangential one by $\mathbf{p}_T = (\mathbf{1} - \mathbf{n} \otimes \mathbf{n})\mathbf{p} = \mathbf{p} - p_N\mathbf{n}$, $\mathbf{p}$ is the total contact stress vector, μ_F is the coefficient of friction, $\mathbf{t}$ and $\mathbf{n}$ are the unit vectors tangential (in the direction of slip) and normal to the contact surface, respectively and $\otimes$ denotes the tensor product of two vectors. The friction coefficient is determined by Eq. (4).

By limiting the maximum shear force transmitted through the joint, the coefficient of friction defines the position at which the tangential loading stops and the plastic slip occurs. The plastic-slip occurs when the shear stress increment p_T acting at contact surface exceeds the limiting value of $\mu_F|p_N|$.

The following additive equations are assumed for the incremental elasto-plastic sliding model

$$\begin{aligned} \Delta u_T &= \Delta u_T^{\mathrm{e}} + \Delta u_T^{\mathrm{p}}, \\ \Delta u_N &= \Delta u_N^{\mathrm{e}} + \Delta u_N^{\mathrm{p}}, \end{aligned} \tag{6}$$

in which the contact displacements denoted by 'e' corresponds to the elastic (reversible) part and 'p' one to the plastic (irrevesible) part. The constitutive law for the elastic part of the displacements corresponds to the negative value of the sliding function F (see Eq. (5)) while the constitutive relationship between the contact displacements and contact stresses can be expressed by

$$\left\{ \begin{array}{c} \Delta p_T \\ \Delta p_N \end{array} \right\} = \mathbf{E}_c^{\mathrm{e}} \left\{ \begin{array}{c} \Delta u_T \\ \Delta u_N \end{array} \right\} = \left[\begin{array}{cc} k_T^{\mathrm{e}} & 0 \\ 0 & k_N^{\mathrm{e}} \end{array} \right] \left\{ \begin{array}{c} \Delta u_T \\ \Delta u_N \end{array} \right\}, \tag{7}$$

in which k_T^{e} and k_N^{e} are the coefficients of the constitutive elastic diagonal martix $\mathbf{E}_c^{\mathrm{e}}$ obtained from Eqs. (3) and (2), respectively.

The plastic contact incremental displacement $\Delta\mathbf{u}^{\mathrm{p}} = \{\Delta u_T^{\mathrm{p}}, \Delta u_N^{\mathrm{p}}\}$ is calculated by adopting a non-associated interface contact stress potential in the form

$$\Delta\mathbf{u}^{\mathrm{p}} = \Delta\lambda \frac{\partial G}{\partial \mathbf{p}}. \tag{8}$$

Adopting the associated slip law in which $G = F$ would yield as a rule a non-zero value for the uplifting normal incremental plastic displacement Δu_N^{p} (which is due to the dilatancy phenomena — thickening of an interface due to the larger volume of space ocuppied by the rubbled asperity material relativy to its initial, intact volume). Since such behaviour for metallic bodies finds no experimental support [18, 40, 41], a non-associated slip law should be adopted in which $F \neq G$. The non-associated slip rule is considered in the following investigation by setting $\Delta u_N^{\mathrm{p}} \equiv 0$, [18, 46]. The plastic/slip potential G, whose gradient gives the direction of the slip, is assumed as

$$G = \|\mathbf{p}_T\|. \tag{9}$$

The plastic displacements are then obtained as follows

$$\Delta u_T^{\mathrm{p}} = \Delta\lambda \frac{\partial G}{\partial p_T} = \Delta\lambda \,\mathrm{sign}(p_T). \tag{10}$$

The elastic domain is defined by an updated sliding surface $F(p_T, p_N, \mu_F) \leq 0$. Loading and unloading conditions may by expressed by requiring that

$$F(\mathbf{p}, \mu_F) \leq 0, \qquad \Delta\lambda \geq 0, \qquad \Delta\lambda\, F(\mathbf{p}, \mu_F) \equiv 0. \tag{11}$$

These are the so-called Kuhn-Tucker unilateral constraints conditions. Note that if $F < 0$ then $\Delta\lambda = 0$ and the sliding surface F is not active (sticking contact). If $\Delta\lambda > 0$ then $F = 0$ and the sliding surface F is active. In the latter case $\Delta\lambda$ is a proportionality factor known as the plastic/slip multiplier which is determined by requiring that $\Delta F = 0$ (the so-called consistency condition). From the above condition we get

$$\Delta F = \frac{\partial F}{\partial p_T}\Delta p_T + \frac{\partial F}{\partial p_N}\Delta p_N + \frac{\partial F}{\partial \mu_F}\frac{\partial \mu_F}{\partial \overline{u_T^{\mathrm{p}}}}\frac{\partial \overline{u_T^{\mathrm{p}}}}{\partial u_T^{\mathrm{p}}}\Delta u_T^{\mathrm{p}} = 0. \tag{12}$$

From (12) and (10) the plastic/slip multiplier is given as

$$\Delta\lambda = \frac{\dfrac{\partial F}{\partial p_T}\Delta p_T + \dfrac{\partial F}{\partial p_N}\Delta p_N}{-\dfrac{\partial F}{\partial \mu_F}\dfrac{\partial \mu_F}{\partial \overline{u_T^{\mathrm{p}}}}\dfrac{\partial \overline{u_T^{\mathrm{p}}}}{\partial u_T^{\mathrm{p}}}\dfrac{\partial G}{\partial p_T}}, \tag{13}$$

while from (4)

$$\frac{\partial \mu_F}{\partial \overline{u_T^{\mathrm{p}}}} = n\mu_m(1-\beta)\exp\left(-n\overline{u_T^{\mathrm{p}}}\right). \tag{14}$$

Taking into account that

$$\frac{\partial F}{\partial p_T} = \frac{\partial G}{\partial p_T} = \operatorname{sign}(p_T), \qquad \frac{\partial F}{\partial p_N} = \mu_F, \qquad \frac{\partial F}{\partial \mu_F} = p_N, \qquad \frac{\partial \overline{u_T^{\mathrm{p}}}}{\partial u_T^{\mathrm{p}}} = \operatorname{sign}(u_T^{\mathrm{p}}), \tag{15}$$

by (13), (14) and (10) $\Delta\lambda$ can be rewritten as

$$\Delta\lambda = \frac{\Delta p_T \operatorname{sign}(p_T) + \mu_F \Delta p_N}{-p_N \mu_m n(1-\beta)\exp\left(-n\overline{u_T^{\mathrm{p}}}\right)\operatorname{sign}(p_T)\operatorname{sign}(u_T^{\mathrm{p}})}, \qquad p_N < 0. \tag{16}$$

Equation (16) is nonlinear with respect to $\Delta\lambda$ which leads to a local iteration procedure to solve (16). In our case the *regula-falsi* was used with normally 3–4 iterations sufficient to reach convergence in practical computations.

For $\Delta\lambda$ known the accumulated (effective) plastic slip is given by

$$\left(\overline{u_T^{\mathrm{p}}}\right)_{n+1} = \left(\overline{u_T^{\mathrm{p}}}\right)_n + \|\Delta \mathbf{u}_T^{\mathrm{p}}\| = \left(\overline{u_T^{\mathrm{p}}}\right)_n + \Delta\lambda, \tag{17}$$

where n denotes the global iteration counter.

By substituting (16), (10) and (7) into (6) and by assuming that $u_N^{\mathrm{p}} = 0$, we have

$$\begin{Bmatrix} \Delta u_T \\ \Delta u_N \end{Bmatrix} = \begin{Bmatrix} \Delta u_T^{\mathrm{e}} \\ \Delta u_N^{\mathrm{e}} \end{Bmatrix} + \begin{Bmatrix} \Delta u_T^{\mathrm{p}} \\ 0 \end{Bmatrix} = [\mathbf{E}_C^{\mathrm{e-p}}]^{-1} \begin{Bmatrix} \Delta p_T \\ \Delta p_N \end{Bmatrix}, \tag{18}$$

where the inverse elasto-plastic interface matrix $[\mathbf{E}_C^{\mathrm{e-p}}]^{-1}$ is given as

$$[\mathbf{E}_C^{\mathrm{e-p}}]^{-1} = \begin{bmatrix} \frac{1}{k_T^{\mathrm{e}}} & 0 \\ 0 & \frac{1}{k_N^{\mathrm{e}}} \end{bmatrix} + \frac{1}{-p_N \dfrac{\partial \mu_F}{\partial \overline{u_T^{\mathrm{p}}}}\operatorname{sign}(p_T)\operatorname{sign}(u_T^{\mathrm{p}})} \begin{bmatrix} \operatorname{sign}(p_T)\operatorname{sign}(p_T) & \mu_F \operatorname{sign}(u_T^{\mathrm{p}}) \\ 0 & 0 \end{bmatrix}. \tag{19}$$

After inversion of the flexibility matrix in Eq. (19), the constitutive interface relationship can be expressed in the form

$$\begin{Bmatrix} \Delta p_T \\ \Delta p_N \end{Bmatrix} = \mathbf{E}_C^{\mathrm{e-p}} \begin{Bmatrix} \Delta u_T \\ \Delta u_N \end{Bmatrix}, \tag{20}$$

in which the expression for the constitutive elasto-plastic interface matrix $\mathbf{E}_C^{\mathrm{e-p}}$ is given by

$$\mathbf{E}_C^{\mathrm{e-p}} = \begin{bmatrix} k_T^{\mathrm{e}} - \alpha \dfrac{(k_T^{\mathrm{e}})^2}{k_T^{\mathrm{e}} - \frac{\partial F}{\partial \mu_F}\frac{\partial \mu_F}{\partial u_T^{\mathrm{p}}}\operatorname{sign}(p_T)\operatorname{sign}(u_T^{\mathrm{p}})} & \alpha \dfrac{-k_T^{\mathrm{e}} k_N \frac{\partial F}{\partial p_N}\operatorname{sign}(p_T)}{k_T^{\mathrm{e}} - \frac{\partial F}{\partial \mu_F}\frac{\partial \mu_F}{\partial u_T^{\mathrm{p}}}\operatorname{sign}(p_T)\operatorname{sign}(u_T^{\mathrm{p}})} \\ 0 & k_N \end{bmatrix}, \tag{21}$$

where α equals 0 or 1 depending on local loading/unloading behaviour.

As a consequence of the non-associated slip rule the constitutive matrix (21) is non-symmetric, and does not easily fit into existing finite elements codes. Pande and Pietruszczak [27] proposed a very attractive method for obtaining a symmetric formulation in the case of non-associated plasticity, which may also turn out effective for solving the non-associated contact problem. Another possibility to avoid non-symmetric interface matrix may be achieved by assuming the normal contact stresses as known (see Eq. (21)) which implies automatically the associated slip rule [40]. This approach leads to a two-step algorithm. In the first step, the normal contact stresses are solved for and in the second one the frictional stresses due to the known normal stresses are calculculated. Such an algorithm needs as a rule a considerable number of iterations to ensure convergence. The latter algorithm was used in the present study.

3. Finite element formulation

3.1. Geometric mapping of the interface element [3, 29, 36]

We consider a two-dimensional problem with two bodies in contact. Each of the bodies is discretized into quadratic continuum finite elements, and the contact surfaces are discretized into quadratic interface elements. One such element, together with geometry of the reference element, is shown in Fig. 1. Since the interface element is restricted to small displacement analysis, only one face of the element is required to define the geometry of the element. The global coordinates of the bottom face of the interface element connected with the body B are given parametrically in terms of the reference geometry shown in Fig. 1 and the reference (or natural) coordinate ξ by the mapping

$$\begin{Bmatrix} x^B \\ y^B \end{Bmatrix} = \begin{bmatrix} N_1 & 0 & N_2 & 0 & N_3 & 0 \\ 0 & N_1 & 0 & N_2 & 0 & N_3 \end{bmatrix} \begin{Bmatrix} \mathbf{x}^B \\ \mathbf{y}^B \end{Bmatrix} \tag{22}$$

with the shape functions given by

$$N_1 = \frac{1}{2}\xi(1-\xi), \qquad N_2 = 1-\xi^2, \qquad N_3 = \frac{1}{2}\xi(\xi+1). \tag{23}$$

These are the shape functions of the eight node serendipity element reduced by assuming $\eta = -1$ for body A or $\eta = +1$ for body B.

Expressions for x^A and y^A are identical to Eq. (22) except that B is replaced by A.

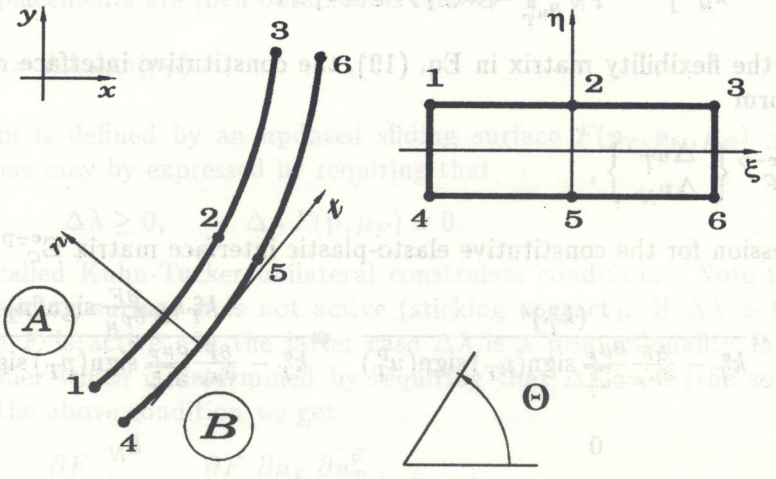

Fig. 1. Geometry of quadratical 6-noded interface element. Geometry of reference element

The unit vectors $\mathbf{t}$ and $\mathbf{n}$ tangential and normal to the contact surface are given in terms of the slope s by, respectively,

$$\mathbf{t} = \frac{\mathbf{i} + s\mathbf{j}}{\sqrt{1+s^2}}, \qquad \mathbf{n} = \frac{-s\mathbf{i} + \mathbf{j}}{\sqrt{1+s^2}}, \tag{24}$$

where $\mathbf{i}$ and $\mathbf{j}$ are the unit vectors in the global x and y directions, respectively, and

$$s = \tan\theta = \frac{N_{,\xi}\,\mathbf{y}^B}{N_{,\xi}\,\mathbf{x}^B}. \tag{25}$$

The kinematic variables used in the constitutive law are the relative surface displacements in the tangential and normal directions that are defined as

$$u_T = (\mathbf{u}^B - \mathbf{u}^A)\mathbf{t}, \qquad u_N = (\mathbf{u}^B - \mathbf{u}^A)\mathbf{n}, \tag{26}$$

where $\mathbf{u}^A$ and $\mathbf{u}^B$ are the displacement vectors of the points associated with the bodies A and B, respectively.

Eqs $(26)_1$ and $(26)_2$ can be rewritten as

$$\begin{aligned} u_T &= (u_x^B - u_x^A)\mathbf{it} + (u_y^B - u_y^A)\mathbf{jt}, \\ u_N &= -(u_x^B - u_x^A)\mathbf{in} + (u_y^B - u_y^A)\mathbf{jn}, \end{aligned} \tag{27}$$

in which $\mathbf{it} = \cos\theta = c$, $\mathbf{jt} = \sin\theta = s$, $\mathbf{in} = -\sin\theta = -s$, $\mathbf{jn} = \cos\theta = c$.

Combining Eqs. (23) to (27) yields

$$\begin{Bmatrix} u_T \\ u_N \end{Bmatrix} = \begin{bmatrix} -c & c & -s & s \\ s & -s & -c & c \end{bmatrix} \begin{Bmatrix} u_x^A \\ u_x^B \\ u_y^A \\ u_y^B \end{Bmatrix}, \tag{28}$$

so that we arrive at

$$\begin{Bmatrix} u_T \\ u_N \end{Bmatrix} = \mathbf{B}\left[u_{1x}, u_{1y}, u_{2x}, u_{2y}, u_{3x}, u_{3y}, u_{4x}, u_{4y}, u_{5x}, u_{5y}, u_{6x}, u_{6y}\right]^T, \tag{29}$$

where $\mathbf{B} = \mathbf{TM}$ with

$$\mathbf{T} = \begin{bmatrix} -c & c & -s & s \\ s & -s & -c & c \end{bmatrix} \tag{30}$$

and

$$\mathbf{M} = \begin{bmatrix} N_1 & 0 & N_2 & 0 & N_3 & 0 & 0 & 0 & 0 & 0 & 0 & 0 \\ 0 & 0 & 0 & 0 & 0 & 0 & -N_1 & 0 & -N_2 & 0 & -N_3 & 0 \\ 0 & N_1 & 0 & N_2 & 0 & N_3 & 0 & 0 & 0 & 0 & 0 & 0 \\ 0 & 0 & 0 & 0 & 0 & 0 & 0 & -N_1 & 0 & -N_2 & 0 & -N_3 \end{bmatrix}. \tag{31}$$

3.2. Incremental description of the contact problem

We have indicated that for an effective numerical treatment of problems involving material non-linearities and the irreversible nature of friction it is necessary to use an incremental formulation. We consider the contact problem in which the contact area during the load increment is assumed known. For the small deformation, elasto-plastic contact problem the fundamental systems of incremental equations can be written in the form

$$(\mathbf{K}_{AB}^{\mathrm{E-P}} + \mathbf{K}_C(\mathbf{u}))\Delta\mathbf{u} = \mathbf{Q} - \mathbf{F} - \mathbf{F}_C \tag{32}$$

where $\mathbf{K}_{AB}^{\mathrm{E-P}}$ is the elastic-plastic stiffness matrix given as

$$\mathbf{K}_{AB}^{\mathrm{E-P}} = \int_{V_{AB}} \mathbf{B}_{AB}^T \mathbf{C}^{\mathrm{E-P}} \mathbf{B}_{AB} \, \mathrm{d}V \tag{33}$$

in which $\mathbf{C}^{\mathrm{E-P}}$ is referred to as the elasto-plastic constitutive tensor as presented in Kleiber [21] or Hinton and Owen [15], for instance, $\mathbf{Q}$ is the vector of the external equivalent nodal load, $\mathbf{F}$ is the vector of the internal nodal forces (without the contact nodes) related to the element stresses $\boldsymbol{\sigma}$ by

$$\mathbf{F} = \int_{V_{AB}} \mathbf{B}_{AB}^T \boldsymbol{\sigma} \, \mathrm{d}V \tag{34}$$

and $\mathbf{B}_{AB}$ is the strain–displacement matrix. $\mathbf{K}_{AB}^{\mathrm{E-P}}$ and $\mathbf{F}$ are evaluated numerically by Gauss integration with 3×3 sampling points. For the path-integration of Eqs. (33) and (34) the explicit method and the subincrementation technique is applied as suggested in [15].

The contact stiffness matrix and the contact force vector are obtained by the standard procedure (the work of equivalent contact forces must be equal to the work of the contact stresses on arbitrary contact displacements). The contact stiffness matrix can be written as follows

$$\mathbf{K}_C^{\mathrm{e-p}} = \int_{A_C} \mathbf{B}^T \mathbf{E}_C^{\mathrm{e-p}} \mathbf{B} \, \mathrm{d}A_C \tag{35}$$

whereas the nodal contact forces $\mathbf{F}_C$ are given by

$$\mathbf{F}_C = \int_{A_C} \mathbf{B}^T \mathbf{p} \, \mathrm{d}A_C \tag{36}$$

in which the matrix $\mathbf{B}$ is given in Eq. (29) and $\mathbf{p}$ denotes the contact stress vector calculated from constitutive friction law (Eq. (20)). Note the analogy between $\mathbf{B}$ and $\mathbf{B}_{AB}$ (the strain–displacement matrix used in conventional formulation of finite elements) except that $\mathbf{B}$ does not involve the differential operators applied to shape functions.

The elementary contact interface area for the axisymmetric case is given as

$$\mathrm{d}A_C = 2\pi r \det \mathbf{j} \, \mathrm{d}\xi \tag{37}$$

where r is the radial distance to the sampling point under consideration and $\det \mathbf{j}$ is the determinant of the transformation Jacobian matrix from global to local coordinates expressed as

$$\det \mathbf{j} = \sqrt{\left(\frac{\partial r}{\partial \xi}\right)^2 + \left(\frac{\partial z}{\partial \xi}\right)^2} \,. \tag{38}$$

3.3. Integration of the contact constitutive relations

3.3.1. Quadrature integration (three-point Newton-Cotes)

For the evaluation of the contact stiffness martix (35) and the corresponding contact load vector (36) some numerical integration scheme needs to be employed. The numerical integration becomes more atractive in the case of curved elements with varying stiffnesses, as encountered in the general case of contact problem with interface compliance. It is known that the performance of the contact elements can depend strongly on the type of integration rule adopted. The full integration (three-point Gauss) proves to yield undesirable oscillations in computed stress results. As shown in Gens et al. [13], Qiu et al. [31], Hohlberg [17], the use of the diagonal or lumped contact stiffness such as those obtained in Newton-Cotes integration, which results in uncoupling of the degrees of freedom, can be very advantageous. In computations involving the quadratic contact element used in our analysis, the results obtained by using the three-point Newton-Cotes integration (Lobatto

rule) were observed to be almost always slighty better (oscillations in stress results reduced) than the results obtained by using the full integration (three-point Gauss rule) [31]. There are several ways to construct lumped-stiffness matrices [19, 44]: the nodal quadrature rules, row-sum technique and special lumping technique. The row-sum technique integration, like the full quadrature, produces sometimes negative contact stiffness coefficient. This is the case for corner nodes of 20-node serendipity element [6]. Such an algorithm makes sense only when all the degrees of freedom have the same physical interpretation. This method has been used successfully in the plane-contact problem by Buczkowski and Kleiber [5]. The special lumping technique was developed by Hinton, Rock and Zienkiewicz [16]. The idea is to set the entries of the lumped coefficient matrix proportional to the diagonal entries of the consistent contact element area. This method always produces positive lumped contact stiffness coefficients. It is only the lumped method that can be recommended for arbitrary contact elements. The special lumping procedure has been used succefully in solid mechanics (lumped masses) by Hinton and Owen [15, 16]. Unfortunately, no mathematical theory in support of it has ever been given. The lumped matrix has clear physical interpretation; it represents the stiffness matrix of a nonlinear spring-contact elements lying between the discrete contact points.

In our analysis Eqs. (35) and (36) have been evaluated by the three-point Newton-Cotes method. The numerical integration of $\mathbf{F}_C$ (Eq. (36)) for the Newton-Cotes with three sampling points (contact points) leads to

$$\mathbf{F}_C = 2\pi \sum_{g=1}^{3} \mathbf{B}^T(\xi_g)\, \mathbf{p}(\xi_g)\, r(\xi_g)\, \det \mathbf{j}(\xi_g)\, W_g\,. \tag{39}$$

If the sampling points of the numerical integration are located at nodes then all the shape functions except N_i are zero at any node i and the matrix becomes diagonal. An integration formula at the contact nodes for submatrix $\mathbf{K}^C_{pq}$ of the contact stiffness matrix $\mathbf{K}^{e-p}_C$ (Eq. (35)) linking the nodes of the top and bottom interface element takes the form (see Fig. 1).

$$\mathbf{K}^C_{pq} = \begin{cases} 2\pi \sum_{g=1}^{3} \mathbf{B}_i(\xi_g)\, \mathbf{E}^{e-p}\, \mathbf{B}_j(\xi_g)\, r(\xi_g)\, \det \mathbf{j}(\xi_g)\, W_g & \text{for } i = j, \\ \mathbf{0} & \text{for } i \neq j. \end{cases} \tag{40}$$

p and q are the element equation numbers; $p \geq 1$ and $q \leq 6$, g refers to the sampling point at which the integral is evaluated, det $\mathbf{j}$ is the determinant of the Jacobian transformation, W_g are the appropriate quadrature weights; $W_1 = 2/6$, $W_2 = 8/6$, $W_3 = 2/6$, ξ_g is the position of integration points; $\xi_1 = -1$, $\xi_2 = 0$, $\xi_3 = 1$, $\mathbf{N}_i = \mathbf{I}N_i$, i runs over 1, 2, 3, and $\mathbf{I}$ is the 2×2 identity matrix.

If three-point Newton-Cotes procedure is used for the axisymmetric analysis zero stiffness coefficient results for the contact point lying on the axis of symmetry. Zero stiffness contact coefficient in the axisymmetric case can be overcome by moving the first interface element beyond the contact node for which $r = 0$.

Remark: When the degrees of freedom are uncoupled and the constraints are employed in a point-wise manner this formulation leads to the penalty finite element method. It should be noted that the penalty finite element method and the mixed finite element method (interpolating contact displacements and contact tractions with independent fields) give identical stress solutions at integration points provided both are numerically-integrated by the same rule [31].

3.3.2. Path integration of the contact stresses

Several integration methods have been used in the literature for elasto-plastic constitutive models. They can be classified as explicit (such as forward Euler) and implicit methods [9, 30, 33, 45]. The limitations of the explicit methods are that the computed stresses may not satisfy the yield criterion at each time interval, and local errors may accumulate. Therefore, subincrements within each time

step are often recommended. The implicit methods (backward Euler, generalized midpoint rule, cutting plan-algorithm, closed point projection) are usually based on the return mapping concept originally proposed in 1964 by Wilkins. In such an approach stresses are updated in two steps. First the elastic (or trial) stress predictor is evaluated, which is subsequently relaxed into an updated yield surface (plastic corrector). Such a plastic relaxation process is completed as soon as the yield condition is fullfilled. The combination of the frictional interface law with the radial return mapping was first used by Wriggers [40] and extended by Wriggers et al. [41]. A similar approach was presented by Giannakopoulos [14]. In this study the radial return method is adopted as well; Box 1 presents the corresponding flow-diagram of the integration process for our contact model. The problem is solved incrementally; from a known state (displacements, stresses) denoted by the subscript (n) we wish to find these quantities at the state $(n+1)$.

Box 1. Radial return algorithm for 2D-contact friction problem

1. Known: p_{T_n} , p_{N_n} , λ_n
2. Elastic predictor phase

   compute trial stress increment

$$\Delta p_T^{(tr)} = k_T^e \Delta u_T$$
$$\Delta p_N = k_N \Delta u_N$$

   compute trial contact stresses

$$p_{T_{n+1}}^{(tr)} = p_{T_n}^{(tr)} + \Delta p_T^{(tr)}$$
$$p_{N_{n+1}} = p_{N_n} + \Delta p_N$$
$$F_{n+1}^{(tr)} = \|p_{T_{n+1}}^{(tr)}\| + \mu_F p_{N_{n+1}}$$

3. Check sliding condition:

   IF $(F_{n+1}^{(tr)} \leq 0)$ THEN

$$p_{T_{n+1}} = p_{T_{n+1}}^{(tr)} \quad \text{(stick, elastic process)}$$

   ELSE (return map)

4. Plastic (friction) corrector phase

   calculate multiplier plastic/slip increment $\Delta\lambda$ from Eq. (16)

$$p_{T_{n+1}} = \mu_F p_{N_{n+1}} \frac{p_{T_{n+1}}^{(tr)}}{\|p_{T_{n+1}}^{(tr)}\|}$$

   ENDIF

5. Update

$$\lambda_{n+1} = \lambda_n + \Delta\lambda$$

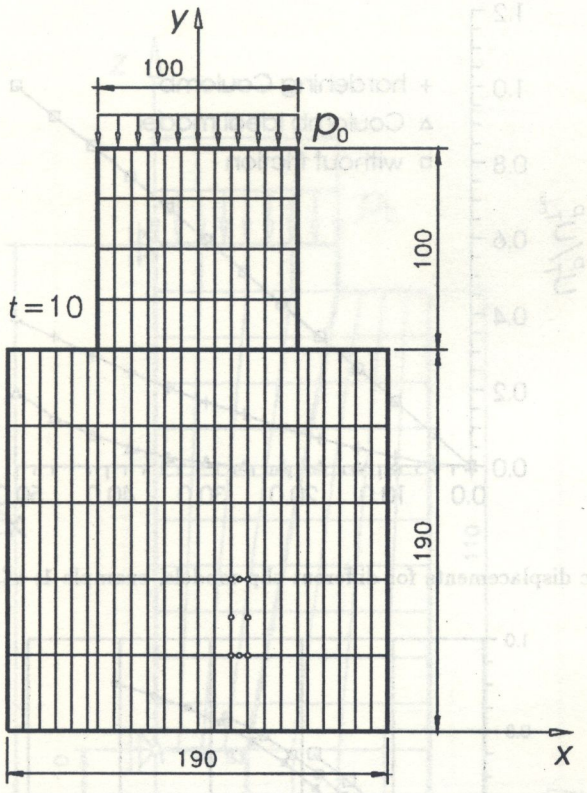

Fig. 2. Plane elastic punch on elastic foundation

4. NUMERICAL EXAMPLES

4.1. Plane elastic punch on an elastic foundation (Fig. 2)

In order to study the effect of the contact properties on the relative plastic displacements for different slip rules an elastic punch acting on an elastic foundation is analysed first. The uniform pressure of $p_0 = 1.2\,[\mathrm{N/mm^2}]$ is applied to the upper face of the punch. The elastic moduli for both the bodies are assumed to be $4000\,[\mathrm{N/mm^2}]$ while the Poisson ratio is 0.35. The contact parameters are assumed as $\mu_m = 0.2$, $\beta = 0.2$, n=275 [1/mm]. Our results are compared with the results of Fredriksson [12]. The results agree very well with the ones obtained there. The amount of slip for different slip rules is shown in Fig. 3. It can be seen that the slip is greater for the slip hardening model than it is for the ideal Coulomb model with the same maximum value of the coefficient of friction. The frictional properties have a great influence on the amount of slip. The hardening model gives higher values of plastic displacements then the ideal Coulomb model. The value of $u^{\mathrm{p}}_{T\max}$ as given by Fredriksson was taken as $10.4\,[\mu\mathrm{m}]$. The variation of the friction coefficient μ_F (see Eq. (4)) with the plastic displacements for the different slip models is given in Fig. 4.

4.2. Tapered joint (Fig. 5)

Due to the geometry of the tapered joints tangential forces carry in them a large part of the loading as compared with the flat joints. An important advantage of the tapered joint is a possibility of controling the pressure on the tapered surface of the joint dependent on the axial force necessary for pushing in a shaft in the sleeve opening. In this case it is of great importance to know the influence of the contact stiffness on the axial displacement. It should be noted that a surplus, fixed value of axial displacement depending on the surface roughnesses is added to calculated theoretical value of axial displacement to take into account plastic deformations of peaks of the asperities of

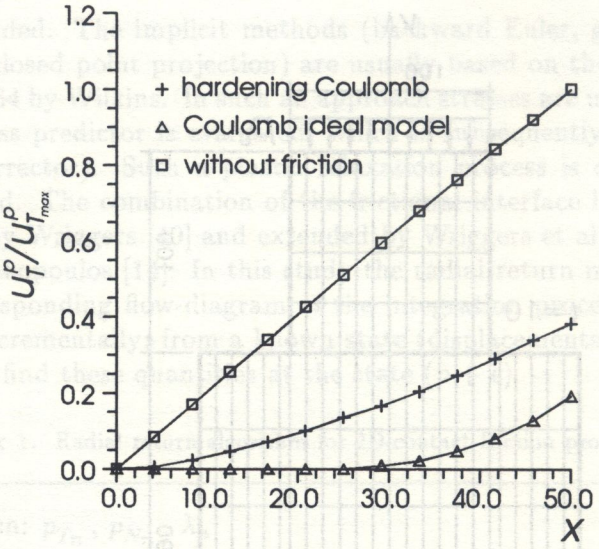

Fig. 3. Plastic displacements for different slip models, example 1; $u^{\mathrm{P}}_{T\max} = 10.8\,[\mu\mathrm{m}]$

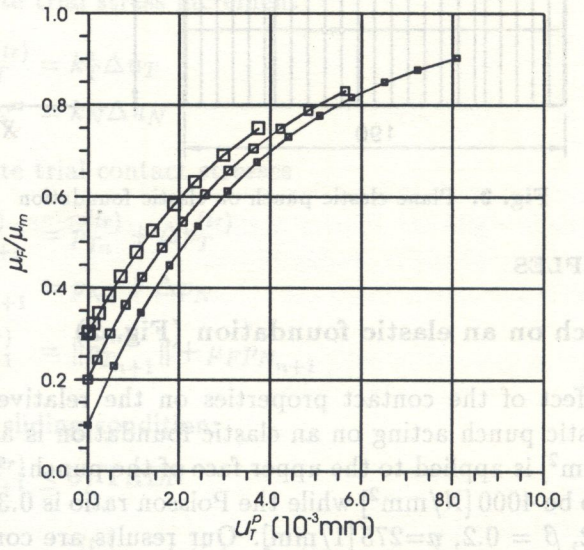

Fig. 4. Variation of friction coefficient μ_F with plastic displacements for different slip models; $\mu_m = 0.1$, $\beta = 0.1$ (small squares), $\mu_m = 0.2$, $\beta = 0.2$ (middle squares), $\mu_m = 0.3$, $\beta = 0.3$ (big squares). $c_N = 0.0001$, $m = 0.5$, $R = 0.5$, $S = 0.5$

the shaft and sleeve [22]. The relationships between the applied forces and the axial displacements were calculated for the taper of 1/2.5. The results are shown in Figure 6. For the purpose of comparison, analytical results of Kollmann [22] are also given. The full line indicates the analytical solution by Kollmann [22] which was obtained without considering the contact stiffness and by assuming the Coulomb ideal friction model. In both the cases the axial displacements are a linear function of the applied force. Next, the same problem was considered with the contact stiffness and friction properties of the contact surface ($\mu_m = 0.2$, $\beta = 1.0$, $n = 275$, $R = 1.0$, $S = 0.5$). Figure 6 shows the nonlinear relationship (the axial displacements as a function of the axial applied forces) for results with the contact stiffness. The difference between the two curves (with different c_N parameters) gradually increases with the increase of the normal contact stiffness of the joint. As sugested by Taniguchi et al. [38] the sufficiently accurate results may be obtained without considering the contact stiffness if the maximum approach of the contact surface is less than half of the sum of the height of surface asperity of both the bodies. In other cases, in the analysis of the axial displacements of the tapered joints it is necessary to introduce the contact stiffness.

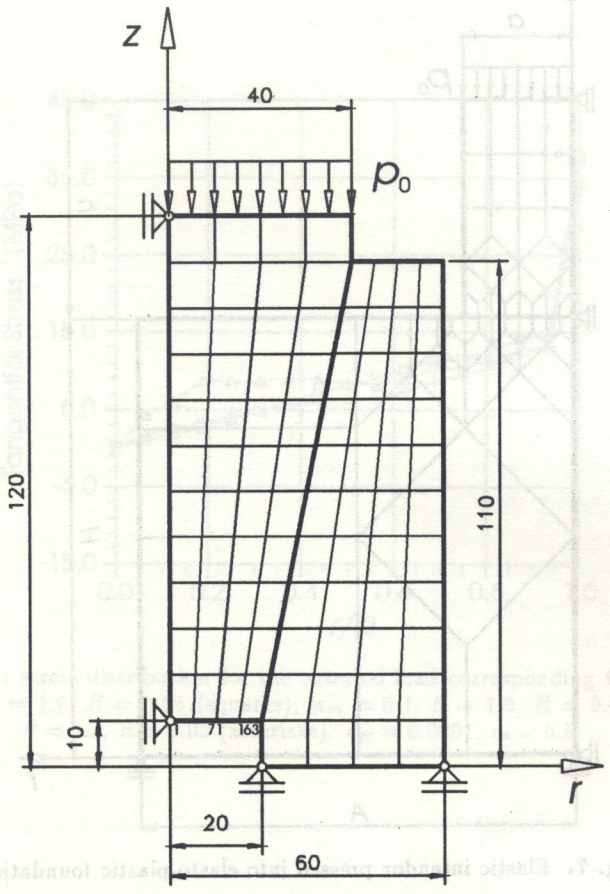

Fig. 5. Model of tapered joint; $E_A = E_B = 2.1 * 10^6$, $\nu_A = \nu_B = 0.3$, $p_0 = 10\,\mathrm{N/mm^2}$

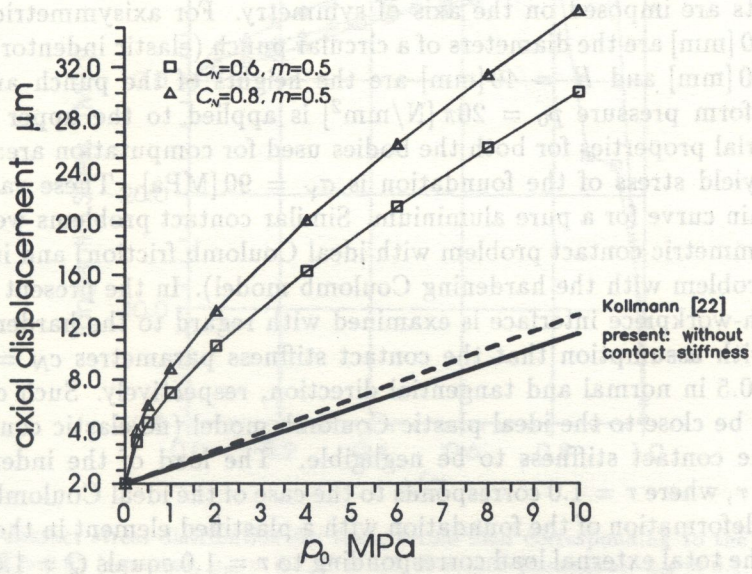

Fig. 6. Influence of contact stiffness parameters on axial displacements compared with the analytical solution of Kollmann [22]. The axial displacements obtained as the average value of the nodal displacements 1, 71 and 163 (see Fig. 5)

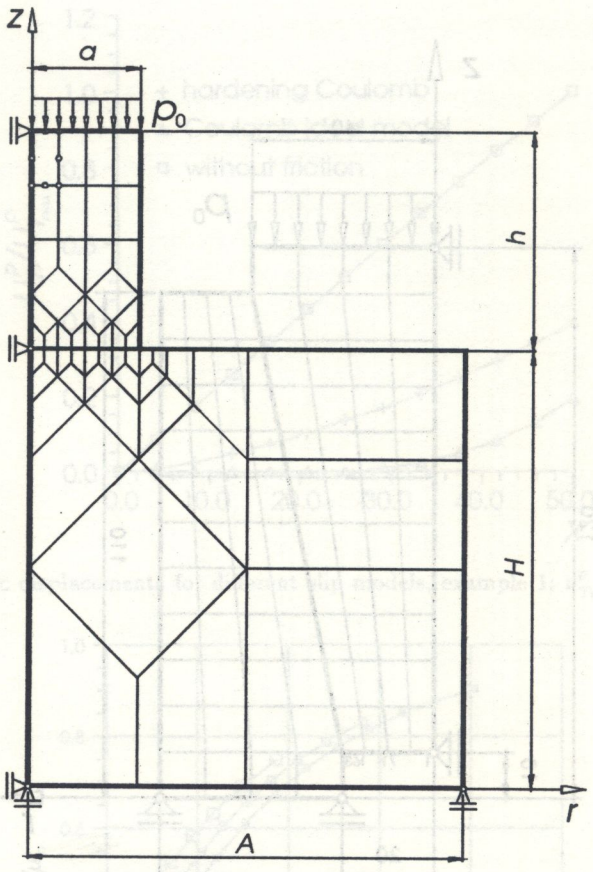

Fig. 7. Elastic intendor pressed into elasto-plastic foundation

4.3. Indentation of axisymmetric punch into elasto-plastic foundation

An elastic punch is pressed against an elasto-plastic foundation as shown in Fig. 7. The appropriate boundary constraints are imposed on the axis of symmetry. For axisymmetric indentation $2a = 20\,[\text{mm}]$ and $2A = 80\,[\text{mm}]$ are the diameters of a circular punch (elastic indentor) and a foundation, respectively, $h = 20\,[\text{mm}]$ and $H = 40\,[\text{mm}]$ are the heights of the punch and the foundation, respectively. A uniform pressure $p_0 = 20\pi\,[\text{N/mm}^2]$ is applied to the upper face of the elastic indentor. The material properties for both the bodies used for computation are: $E = 70000\,[\text{MPa}]$, $\nu = 0.33$, and the yield stress of the foundation is $\sigma_Y = 90\,[\text{MPa}]$. These values correspond to the static stress-strain curve for a pure aluminium. Similar contact problems were analyzed in [35] (elasto-plastic axisymmetric contact problem with ideal Coulomb friction) and in [5] (elasto-plastic plane rigid punch problem with the hardening Coulomb model). In the present paper the effect of friction at the punch-workpiece interface is examined with regard to the hardening friction model (see Eq. (4)) and with assumption that the contact stiffness parametres $c_N = 0.0001$, $m = 0.5$, and $R = 0.05$, $S = 0.5$ in normal and tangential direction, respectively. Such contact parameters cause the friction to be close to the ideal plastic Coulomb model (no elastic contact displacements are allowed) and the contact stiffness to be negligible. The load of the indentor is given by a dimensionless factor r, where $r = 1.0$ corresponds to the case of the ideal Coulomb model with $\mu_m = 0.2$ and the state of deformation of the foundation with a plastified element in the neighbourhood of the punch corner. The total external load corresponding to $r = 1.0$ equals $Q = 1.6\pi a^2 p_0\,[\text{N}]$. Figures 8 and 9 show the tangential stress distributions along the contact surface for different friction models: (a) ideal Coulomb model ($\mu_m = 0.1$, $\beta = 1.0$, $R = 0.05$), (b) regularized (elastic contact displacements included) Coulomb model ($\mu_m = 0.1$, $\beta = 1.0$, $R = 1.0$), (c) hardening Coulomb model ($\mu_m = 0.1$, $\beta = 0.1$, $R = 0.05$). In the three cases (Fig. 9) a decrease of tangential stresses is

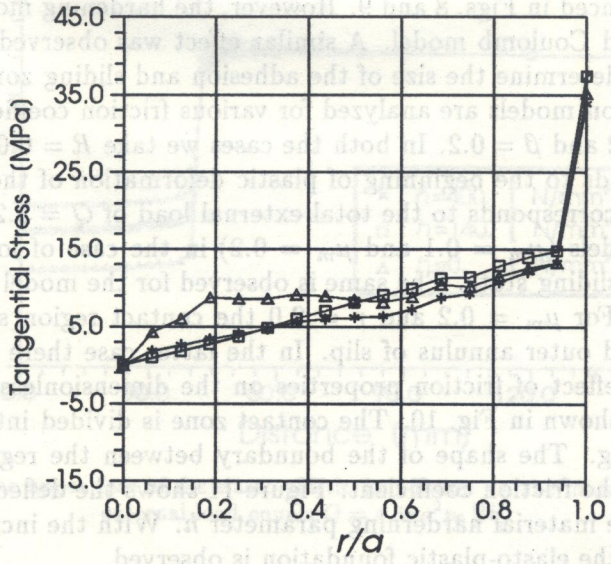

Fig. 8. Tangential contact stress distribution for the external load corresponding to initiation of the plastic deformation; $\mu_m = 0.1$, $\beta = 1.0$, $R = 0.05$ (squares); $\mu_m = 0.1$, $\beta = 1.0$, $R = 0.05$ (triangles); $\mu_m = 0.1$, $\beta = 0.1$, $R = 0.05$ (asterisks). $c_N = 0.0001$, $m = 0.5$

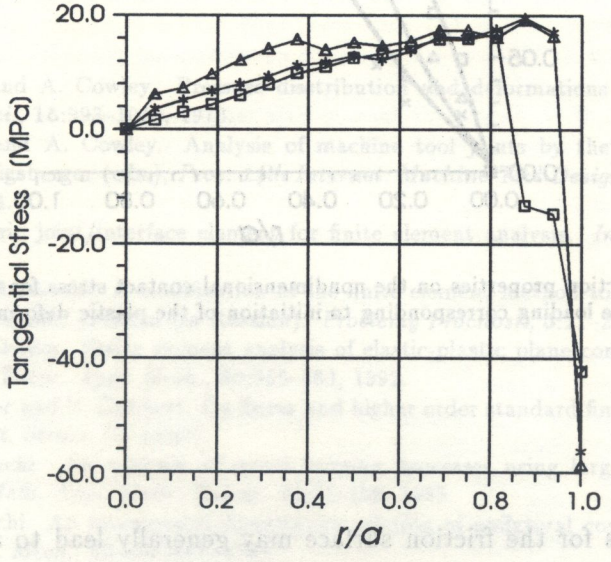

Fig. 9. Tangential contact stress distribution for the external load corresponding to the load factor $r = 2$; $\mu_m = 0.1$, $\beta = 1.0$, $R = 0.05$ (squares); $\mu_m = 0.1$, $\beta = 1.0$, $R = 0.05$ (triangles); $\mu_m = 0.1$, $\beta = 0.1$, $R = 0.05$ (asterisks). $c_N = 0.0001$, $m = 0.5$

observed as the load of the indentor increases, including the change in sign of the tangential stresses. It results from the present analysis that the tangential contact stresses are rather insensitive to the different slip models — only small differences are detected between the results obtained in cases (a), (b), and (c), as evidenced in Figs. 8 and 9. However, the hardening model extends the slip zone more then the regularized Coulomb model. A similar effect was observed in the case of the plane contact problem [5]. To determine the size of the adhesion and sliding zones as a function of load, next two hardening friction models are analyzed for various friction coefficients, i.e.: (1) $\mu_m = 0.1$, $\beta = 0.1$ and (2) $\mu_m = 0.2$ and $\beta = 0.2$. In both the cases we take $R = 0.05$ and $S = 0.5$. The first case of loading corresponds to the beginning of plastic deformation of the foundation, the second one is for $r = 2.0$ which corresponds to the total external load of $Q = 3.2\pi a^2 p_0$ [N]. It is observed for both the friction models ($\mu_m = 0.1$ and $\mu_m = 0.2$) in the case of lower loading that all the contact nodes are in the sliding state. The same is observed for the model with the smaller friction coefficient ($\mu_m = 0.1$). For $\mu_m = 0.2$ and $r = 2.0$ the contact region splits into two parts: an inner adhesive region and outer annulus of slip. In the latter case there are three outer nodes in the sliding region. The effect of friction properties on the dimensionless contact stresses for the ideal Coulomb model is shown in Fig. 10. The contact zone is divided into the region of adhesion and the region of slipping. The shape of the boundary between the region of slip and adhesion depends on the value of the friction coefficient. Figure 11 shows the deflection of the upper face of the foundation versus the material harderning parameter h. With the increase of the parameter h the overall hardening of the elasto-plastic foundation is observed.

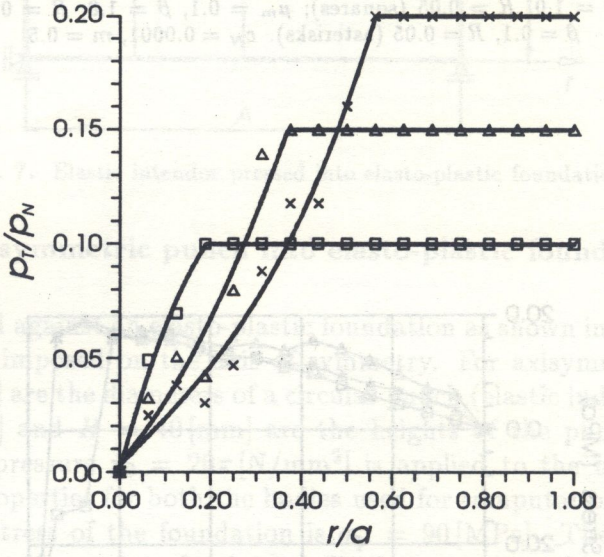

Fig. 10. Effect of the friction properties on the nondimensional contact stress for the ideal Coulomb model and the loading corresponding to initiation of the plastic deformation

5. CONCLUSIONS

1. Constitutive equations for the friction surface may generally lead to an unsymmetric contact stiffness matrix.
2. Symmetrization of the contact stiffness matrix can be obtained by assuming a known value of the contact pressure p_N. This approach leads to a two-step algorithm. In the first step, a solution of the normal contact is found and in the second one the frictional stresses due to the known normal pressure are computed.

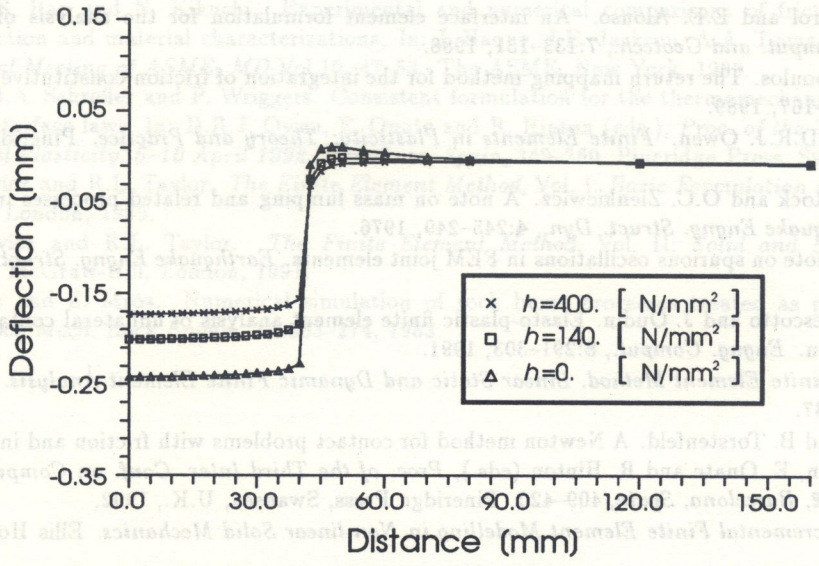

Fig. 11. Deflection of the upper face of the elasto-plastic foundation vs. the material harderning h. Total external load equals $Q = 4.6\pi a^2 p_0$ [N]

3. Because of the ill-conditioned elastic-platic contact stiffness matrix, calculations were carried out using the elastic contact matrix $\mathbf{K}_C^e$ analogous to the initial elastic matrix $(\mathbf{K}_{AB}^E)^0$ in the problem of material elasto-plastic deformations. Even though it results in a longer computation time, it assures stable iterative calculation.

4. When a monotonically increasing load is applied to the cylindrical intendor, the region of contact splits into an inner adhesive region and an outer annulus of inward slip. The radius of adhesion for the regularized Coulomb model is greater than that for the hardening Coulomb model for the same value of the macroscopic friction coefficient.

REFERENCES

[1] N. Back, M. Burdekin and A. Cowley. Pressure disstribution and deformations of machined components in contact. *Int. J. Mech. Sci.*, **15**:993–1010, 1973.

[2] N. Back, M. Burdekin and A. Cowley. Analysis of machine tool joints by the finite element method. In: S.A. Tobias and F. Koenigsberger (eds.), *Proc. 14th Internat. Machine Tool Design and Research Conf.*, 87–97. MacMillan, London, 1974.

[3] G. Beer. An isoparametric joint/interface element for finite element analysis. *Int. J. Num. Methods Engng.*, **21**:585–600, 1985.

[4] M.W. Bloch and M.W. Orobinski. A modification of the finite element method to computation the elastic and plastic two dimensional contact problem (in Russian). *Problemy Pročnosti*, **5**:21–27, 1983.

[5] R. Buczkowski and M. Kleiber. Finite element analysis of elastic-plastic plane contact problem with nonlinear interface compliance. *J. Theor. Appl. Mech.*, **30**:855–883, 1992.

[6] R. Buczkowski, M. Kleiber and U. Gabbert. On linear and higher order standard finite elements for 3D-nonlinear contact problem. *Comput. Struct.* (in print).

[7] J.H. Cheng and N. Kikuchi. An analysis of metal forming processes using large deformation elastic-plastic formulations. *Comput. Meth. Appl. Mech. Engng.*, **49**:71–108, 1985.

[8] J.H. Cheng and N. Kikuchi. An incremental constitutive relation of unilateral contact friction for large deformation analysis. *J. Appl. Mech.*, **52**:639–648, 1985.

[9] M.A. Crisfield. *Non-linear Finite Element Analysis of Solids and Structures.* Vol. 1. *Essentials.* Wiley, Chichester, 1991.

[10] A. Curnier. A theory of friction. *Int. J. Solids Struct.*, **20**:637–647, 1984.

[11] C.S. Desai and Y. Ma. Modelling of joints and interfaces using the distributed-state concept. *Int. J. Num. Anal. Meth. Geomech.*, **16**:623–653, 1992.

[12] B. Fredriksson. Finite element solution of surface nonlinearities in structural mechanics with emphasis to contact and fracture mechanics problems. *Comput. Struct.*, **6**:281–290, 1976.

[13] A. Gens, I. Carol and E.E. Alonso. An interface element formulation for the analysis of soil-reinforcement interaction. *Comput. and Geotech.*, **7**:133–151, 1988.

[14] A.E. Giannakopoulos. The return mapping method for the integration of friction constitutive relations. *Comput. Struct.*, **32**:157–167, 1989.

[15] E. Hinton and D.R.J. Owen. *Finite Elements in Plasticity: Theory and Practice.* Pineridge Press, Swansea, U.K., 1980.

[16] E. Hinton, T. Rock and O.C. Zienkiewicz. A note on mass lumping and related processes in the finite element method. *Earthquake Engng. Struct. Dyn.*, **4**:245–249, 1976.

[17] J. Hohberg. A note on spurious oscillations in FEM joint elements. *Earthquake Engng. Struct. Dyn.*, **19**:773–779, 1990.

[18] P. Hrycaj, S. Cescotto and J. Oudin. Elasto-plastic finite element analysis of unilateral contact with generalized Coulomb friction. *Engng. Comput.*, **8**:291–303, 1991.

[19] Hughes. *The Finite Element Method. Linear Static and Dynamic Finite Element Analysis.* Prentice-Hall Inc., New Jersey, 1987.

[20] A. Klarbring and B. Torstenfeld. A Newton method for contact problems with friction and interface compliance. In: D.R.J. Owen, E. Onate and R. Hinton (eds.), *Proc. of the Third Inter. Conf. on Computational Plasticity, 6–10 April 1992, Barcelona, Spain*, 409–420. Pineridge Press, Swansea, U.K., 1992.

[21] M. Kleiber. *Incremental Finite Element Modelling in Non-linear Solid Mechanics.* Ellis Horwood, Chichester, 1989.

[22] F.G. Kollmann. *Welle-Nabe-Verbindungen; Gestaltung, Auslegung Auswahl.* Springer-Verlag, Berlin, 1984.

[23] L. Kops and D.H. Abrams. Effect of shear stiffness of fixed joints on thermal deformation of machine tools. *Annals of CIRP*, **33**:223–238, 1984.

[24] T.A. Laursen and J.C. Simo. On the formulation and numerical treatment of finite deformation frictional contact problems. In: P. Wriggers and W. Wagner (eds.), *Nonlinear Computational Mechanics, State of the Art*, 716–736. Springer-Verlag, Berlin, 1991.

[25] Z.M. Levina. Research on the static stiffness of joints in machine tools. *Proc. 8th Internat. Machine Tool Design and Research Conf., London*, 737–758. 1965.

[26] R. Michałowski and Z. Mróz. Associated and non-associated sliding rules in contact friction problems. *Arch. of Mech.*, **30**:259–276, 1978.

[27] G.N. Pande and S. Pietruszczak. Symmetric tangential stiffness formulation for non-associated plasticity. *Comput. and Geotech.*, **2**:89–99, 1986.

[28] M.E. Plesha. Constitutive models for rock discontinuities with dilatancy and surface degradation. *Int. J. Numer. Anal. Meth. Geomech.*, **11**:345–362, 1987.

[29] M.E. Plesha, R. Ballarini and A. Parulekar. Constitutive model and finite element procedure for dilatant contact problems. *J. of Engng. Mech., ASCE*, **115**:2649–2668, 1989.

[30] K. Runesson, S. Sture and K. Willam. Integration in computational plasticity. *Comput. Struct.*, **30**:119–130, 1988.

[31] X. Qiu, M.E. Plesha and D.W. Meyer. Stiffness matrix integration rules for contact-friction finite elements. *Comput. Meth. Appl. Mech. Engng.*, **93**:385–399, 1991.

[32] N.J. Salamon, X.X. Tong and F.F. Mahmoud. Effects of profile, roughness and friction on contacting bodies in compression. *Wear*, **101**:205–218, 1985.

[33] J.C. Simo and T.R.J. Hughes. *Elastoplasticity and Viscoplasticity. Computational Aspects*, Springer-Verlag, Berlin (to be published).

[34] J.C. Simo and T.A. Laursen. An augmented lagrangian treatment of contact problems involving friction. *Comput. Struct.*, **42**:97–116, 1992.

[35] K. Skalski. Contact problem in elastic-plastic range (in Polish). In: Z. Mróz (ed.), *Mechanics of Contact Surface*, 211–273. Ossolineum, Wrocław, 1988.

[36] M.F. Snyman, W.W. Bird and J.B. Martin. A simple formulation of a dilatant joint element governed by Coulomb friction. *Engng. Comput.*, **8**:215–229, 1991.

[37] A.G. Tangena and P.J.M. Wijnhoven. Finite element calculations on the influence of surface roughness on friction. *Wear*, **27**:601–607, 1985.

[38] A. Taniguchi, M. Tsutsumi and Y. Ito. Treatment of contact stiffness in structural analysis. *Bull.of the JSME*, **27**:601–607, 1984.

[39] A. Villanueva-Leal and S. Hinduja. Modelling the characteristics of interface by the finite element method. *Proc. Inst. Mech. Engrs.*, **198C**:9–23, 1984.

[40] P. Wriggers. On consistent tangent matrices for frictional contact problems. In: *Proc. of the Conf. NUMETA 87, Swansea*, C15/1–C15/8, 1987.

[41] P. Wriggers, T. Vu-Van and E. Stein. Finite-element-formulation of large deformation impact-contact-problems with friction. *Comput. Struct.*, **37**:319–331, 1990.

[42] B.B. Yao, R.S. Rao and N. Kikuchi. Experimental and numerical comparisons of friction contact in sheet stretching, friction and material characterizations, In: I. Haque, J.E. Jackson, A.A. Tseng and J.L. Rose (eds.) *Winter Annual Meeting of ASME, MD* Vol.10, 47–53. The ASME, New York, 1989.

[43] G. Zavarise, B.A. Schrefler and P. Wriggers. Consistent formulation for the thermomechanical contact based on microscopic interface laws, In: D.R.J. Owen, E. Onate and R. Hinton (eds.), *Proc. of the Third Inter. Conf. on Computational Plasticity, 6–10 April 1992, Barcelona, Spain*, 349–360. Pineridge Press, Swansea, U.K., 1992.

[44] O.C. Zienkiewicz and R.L. Taylor. *The Finite Element Method*, Vol. I: *Basic Formulation and Linear Problems.* McGraw-Hill, London, 1989.

[45] O.C. Zienkiewicz and R.L. Taylor. *The Finite Element Method*, Vol. II: *Solid and Fluid Mechanics and Non-linearity.* McGraw-Hill, London, 1991.

[46] A. Zubelewicz and Z. Mróz. Numerical simulation of rock burst processes treated as problems of dynamic instability. *Rock Mech. Rock Engng.*, **16**:253–274, 1983.